Nanoscale Advances

ROYAL SOCIETY OF CHEMISTRY

PAPER

View Article Online
View Journal | View Issue

Cite this: *Nanoscale Adv.*, 2021, **3**, 3288

Controlling optical trapping of metal–dielectric hybrid nanoparticles under ultrafast pulsed excitation: a theoretical investigation†

Anita Devi, ‡[a] Shruthi S. Nair,‡[bcd] Sumit Yadav [a] and Arijit K. De *[b]

Received 29th December 2020
Accepted 2nd April 2021

DOI: 10.1039/d0na01083a

rsc.li/nanoscale-advances

Crucial to effective optical trapping is the ability to precisely control the nature of force/potential to be attractive or repulsive. The nature of particles being trapped is as important as the role of laser parameters in determining the stability of the optical trap. In this context, hybrid particles comprising of both dielectric and metallic materials offer a wide range of new possibilities due to their tunable optical properties. On the other hand, femtosecond pulsed excitation is shown to provide additional advantages in tuning of trap stiffness through harnessing optical and thermal nonlinearity. Here we demonstrate that (metal/dielectric hybrid) core/shell type and hollow-core type nanoparticles experience more force than conventional core-type nanoparticles under both continuous-wave and, in particular, ultrafast pulsed excitation. Thus, for the first time, we show how tuning both materials properties as well as the nature of excitation can impart unprecedented control over nanoscale optical trapping and manipulation leading to a wide range of applications.

Introduction

Optical trapping with laser tweezers[1] employs highly focused laser beams to achieve a high degree of controlled manipulation of dynamics of particles, of micrometers in size down to as small as single atoms, in a contact free manner. Over decades, efforts have been made to trap a wide variety of dielectric objects including live cells and organelles.[1–8] Contrary to dielectrics, for metals reflectivity causes a significant dominance of scattering force over gradient force;[9] also, absorptivity results in an additional force known as absorption force and is responsible for unwanted thermal effects.[10] Despite this, metallic nanoparticles experience enhanced forces because they have higher polarizability which results from the presence of a large number of free electrons;[11–14] this amplifies the electromagnetic field in the vicinity of the particle and is responsible for the plasmonic effects. Owing to this unique behavior, metallic nanoparticles have widespread application in the field of sensing and detection.[15,16] In particular, silver nanoparticles are amply used in medicine due to their biocompatible and antimicrobial properties.[17,18] Moving ahead, one of the ways to improve the trapping efficiency is by using hybrid particles that comprise both metallic and dielectric materials. These novel materials enable fine-tuning of the optical properties according to the specific needs of the experiment by integrating the properties of both the parent materials.[19–21] These metal–dielectric core–shell particles have other advantages such as improved chemical and physical properties, catalytic properties, improved biocompatibility, *etc.*, which makes them good candidates for bio-conjugated experiments.[22–24] A number of techniques and procedures emerged for fabrication of these particles with a controllable composition and morphology,[25–27] opening up the possibilities of using these particles in the aforementioned wide range of applications.[15–18,22–24]

In this article, we discuss how optical trapping efficiency changes with the nature of metal/dielectric core/shell particles, which consist of an inner core made of metal and an outer shell or covering made of dielectric or *vice versa* as well as hollow-core type nanoparticles as well. Specifically, using the dipole approximation, we show theoretical/numerical results on the role of optical nonlinearity in modulating trapping behavior when femtosecond pulsed excitation is used. Although, in the dipole limit, the nonlinear nature of the optical force/potential in femtosecond laser trapping of dielectric[28–30] and metallic[31,32] nanoparticles was theoretically explored in recent times, the same with hybrid nanoparticles is yet to be explored which we present here. It is worth mentioning here that in a recent study optical manipulation of such particles in a counter-propagating beam geometry was investigated where nonlinear scaling of

[a]*Department of Physical Sciences, Indian Institute of Science Education and Research (IISER) Mohali, Knowledge City, Sector 81, SAS Nagar, Punjab 140306, India*
[b]*Department of Chemical Sciences, Indian Institute of Science Education and Research (IISER) Mohali, Knowledge City, Sector 81, SAS Nagar, Punjab 140306, India*
[c]*Institute of Physical Chemistry, Friedrich-Schiller-University Jena, Helmholtzweg 4, 07743 Jena, Germany*
[d]*Department Functional Interfaces, Leibniz Institute of Photonic Technology (IPHT), Albert-Einstein-Strasse 9, 07745 Jena, Germany. E-mail: akde@iisermohali.ac.in*

† Electronic supplementary information (ESI) available. See DOI: 10.1039/d0na01083a

‡ These authors equally contributed to this work.

optical force with power was shown;[33] this arises naturally from multiphoton processes involving an absorbing core (a gain medium), the emission of which is in resonance with the plasmonic transition in the shell. In contrast, in the present work we choose parameters far from resonance where optical nonlinearity arises explicitly from nonlinear polarizability.[28–32]

Results and discussion

The optical trap is always stable along the radial direction as gradient force is the only contributing force. Along the axial direction, the potential well is anharmonic due to contributions from scattering and absorption forces and is majorly responsible for the instability of the trap. Depending on the degree of anharmonicity of the potential, the ease of ejecting the particle along the axial direction also increases.[28–32] The anharmonicity of the potential well along the axial direction for conventional silver nanoparticles is particle-size dependent and it can be along the negative axial direction due the occurrence of Fano resonance (enhanced forward scattering leading to a negative optical scattering force).[32] Hence, we have restricted the discussion in this paper to axial force/potential which determines the stability of the optical trap which is characterized by the quantity escape potential (U_{esc}, potential barrier to escape trap along the axial direction) but not by the absolute potential (U_{abs}, absolute depth of the potential well); these quantities are evaluated by considering the numerical values of potential at the global minimum ($z = z_0$) and in asymptotic regions ($z \to \pm\infty$): $U_{abs} = U(z \to -\infty) - U_{min}(z = z_0)$ and $U_{esc} = U_{max}(z_0 < z < \infty) - U_{min}(z = z_0)$.[28] A detailed methodology is provided in the accompanied ESI.†

Before discussing the extensive study of the hybrid nanoparticles (with varying the laser parameters such as laser power and focusing *via* numerical aperture (NA) as well as particle parameters such as radius of the core/shell), we compare the force/potential experienced by the hybrid particles to that of conventional particles (*i.e.*, purely metallic or dielectric nanoparticles) to illustrate how advantageous it is to use hybrid particles. We have also included a brief section on the behavior of hollow nanoparticles to provide a clear picture. All numerical studies are performed under both CW and pulsed excitation to emphasize the role of nonlinear effects. All parameters used in the numerical simulations are listed in Table 1.

Comparison of hybrid and conventional nanoparticles

CW excitation

The comparison of the force/potential of conventional dielectric (polystyrene) with metallic–dielectric (silver–polystyrene) nanoparticles is shown in Fig. 1a–d. Similarly, the comparison of conventional silver with dielectric–metallic (polystyrene–silver) nanoparticles is shown in Fig. 1e–h. Fig. 1a shows the force/potential of polystyrene nanoparticles with a radius of 10 nm compared to that of core–shell particles with a silver core with a radius of 5 nm embedded within a polystyrene shell with a thickness of 5 nm (denoted as core–shell (5–10 nm) radius; this convention of denoting the respective core–shell thickness is followed throughout the paper).

The silver–polystyrene hybrid particle experiences considerably enhanced forces compared to conventional polystyrene particles, and the corresponding absolute (U_{abs}; longer double-sided arrow) and escape (U_{esc}; shorter double-sided arrow) potentials are also higher for the hybrid particles (shown in Fig. 1c). Thus, by integrating a silver core within a polystyrene particle, the forces acting on it can be significantly enhanced

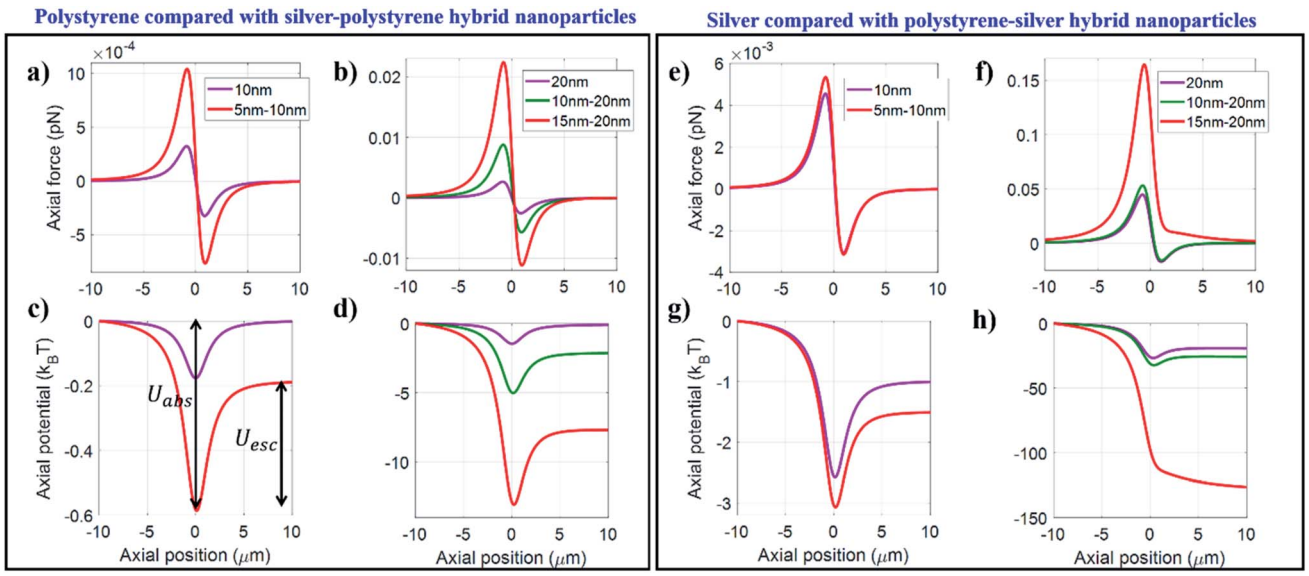

Fig. 1 Plots of trapping force (a and b), potential (c and d) along the axial direction for conventional polystyrene and hybrid silver–polystyrene nanoparticles and trapping force (e and f), potential (g and h) for conventional silver and hybrid polystyrene–silver nanoparticles at 100 mW average power under CW excitation for fixed NA 1.4.

due to the high polarizability of the metallic component of the hybrid particle. Therefore, by accurately controlling the core and shell radius, we can control the force acting on the trapped particle according to our requirement.

The effect of increasing the core size can be seen in Fig. 1b which shows the force/potential for 20 nm polystyrene compared with varying thicknesses of the silver–polystyrene particle: 10–20 nm and 15–20 nm. The force acting on the particle increases with an increasing radius of the silver core, which can be seen from Fig. 1a and b. This can be of major significance while doing bio-conjugated experiments that require a high magnitude of force.[27] Although silver nanoparticles are known for their anti-microbial and anti-cancer properties,[40] they still have the problem of unwanted heating effects that can degrade the samples while using high laser powers. This problem can be circumvented by adding an outer coating of dielectric material that can minimise the absorption or heating effects while utilising the high polarizability of the metallic core. Thus, the choice of outer surface also matters, especially for bio-conjugated samples where we require materials that are bio-compatible while not compromising with the trapping efficiency.

Comparison for 10–20 nm and 15–20 nm polystyrene–silver core–shell particles with 10 nm and 20 nm conventional nanoparticles respectively shows that there is only a slight enhancement in the force/potential as the force on the conventional silver nanoparticle sphere is already high enough. On the other hand, although 15–20 nm particles feel highly enhanced forces compared to 20 nm silver nanoparticles, the potential becomes unbound due to enhanced scattering and absorption forces and thus is not suitable for trapping. Thus, we see that the choice of outer material, the thickness of the outer shell and the inner core are crucial determining factors and should be carefully chosen according to the specific requirements of the experiment. Similarly, along the radial direction, the force/potential is enhanced or diminished depending upon the choice of size/composition of the hybrid particle. As already mentioned, the axial stability of the trap is what ultimately dictates the efficiency of the trap, and the use of hybrid particles increases the axial forces, which improve the trapping efficiency. Along the radial direction, the force may be increased/decreased depending upon the choice of the size/composition of hybrid particles. However, since the trap is always stable along the radial direction, the reduction in the magnitude of force is a minor drawback and, the change in the magnitude of force may be used for fine-tuning the overall force acting the particle.

Pulsed excitation

Under pulsed excitation, the comparison of the force/potential of conventional dielectric (polystyrene) with metallic–dielectric (silver–polystyrene) and conventional metallic (silver) with dielectric–metallic (polystyrene–silver) nanoparticles is shown in Fig. 2a–d and Fig. 2e–h, respectively. Fig. 2a and b correspond to the axial force under pulsed excitation and for different size ratios of silver–polystyrene nanoparticles. The forces are enhanced similar to CW excitation; however, under pulsed excitation, the enhancement is higher in magnitude and can be seen from Fig. 2c and d. However, it has to be kept in mind that both materials have high optical nonlinearity and consequential alteration in the refractive index of the hybrid material can lead to a better or worse modulation of the trapping behaviour depending upon their relative composition and size. Fig. 2e–h indicate that polystyrene–silver with 5–10 nm and 10–20 nm size composition shows a significant enhancement in force. However,

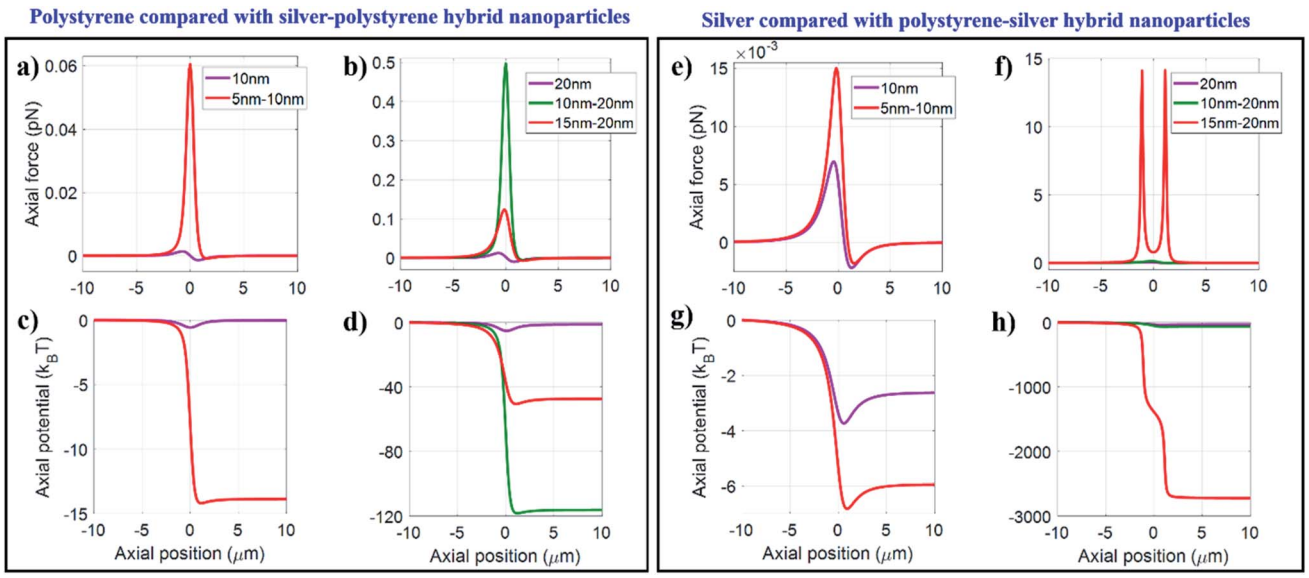

Fig. 2 Plots of trapping force (a–b), potential (c–d) along the axial direction for conventional polystyrene and hybrid silver–polystyrene nanoparticles and trapping force (e–f), potential (g–h) for conventional silver and hybrid polystyrene-silver nanoparticles at 100 mW average power under pulsed excitation for fixed NA 1.4.

15–20 nm shows a splitting nature of the potential well due to the splitting of the absorption force.[31,32] This is because, after a specific size of core particles, plasmonic effects from silver particles dominate. So, the material composition has to be chosen in such a manner that absorption should be minimized. Thus, under pulsed excitation, the choice of shell thickness is crucial and must be chosen judiciously. Under pulsed excitation, the trend observed in radial force/potential is similar to the case of CW excitation; the only difference is in the magnitude of the force/potential, which is more in the case of pulsed excitation.

In previous theoretical work on dielectric and metallic particles from our group,[29–32] we justified that instead of the absolute potential, it is the escape potential that is the appropriate parameter to quantify the stability of the trap. In the ESI,† we provide a detailed theoretical methodology.[31] Fig. S1 in the ESI† shows the plot of the escape potential against the particle size at 100 mW average power under CW excitation for a fixed NA equal to 1.4. Thus, silver particles with a radius of more than 27 nm cannot be trapped due to the dominance of scattering and absorption forces. However, polystyrene particles can be trapped up to 40 nm; beyond this limit we cannot make any comment on trapping of particles since the dipole approximation is not valid anymore.

Hybrid nanoparticles

To generalize these phenomena for hybrid nanoparticles as well, we have rigorously studied the variation in the core and shell size with different NA.

CW excitation

Fig. S2 and S3 in the ESI† show the variation of the escape potential by fixing the shell radius but varying the core radius and *vice versa* respectively for silver–polystyrene nanoparticles at 100 mW average power under CW excitation for different NA. We observe that if we fix the shell/core (metallic/dielectric) radius and vary the core/shell (dielectric/metallic) radius, the maximum radius of the core of a particle that can be trapped is less than 27 nm. This is because above a threshold, the absorption and scattering forces dominate over the gradient force, which results in destabilizing the trap. Adding a dielectric coating on the core does not appear to provide any advantage in terms of improvement in the range of particle size that can be trapped. But it has an advantage in terms of trap stability, which can be seen by comparing Fig. S1 with Fig. S2 & S3.† For example, the escape potential for conventional 20 nm polystyrene nanoparticles is $<2k_BT$, but we can obtain the escape potential $>2k_BT$ for hybrid nanoparticles under similar

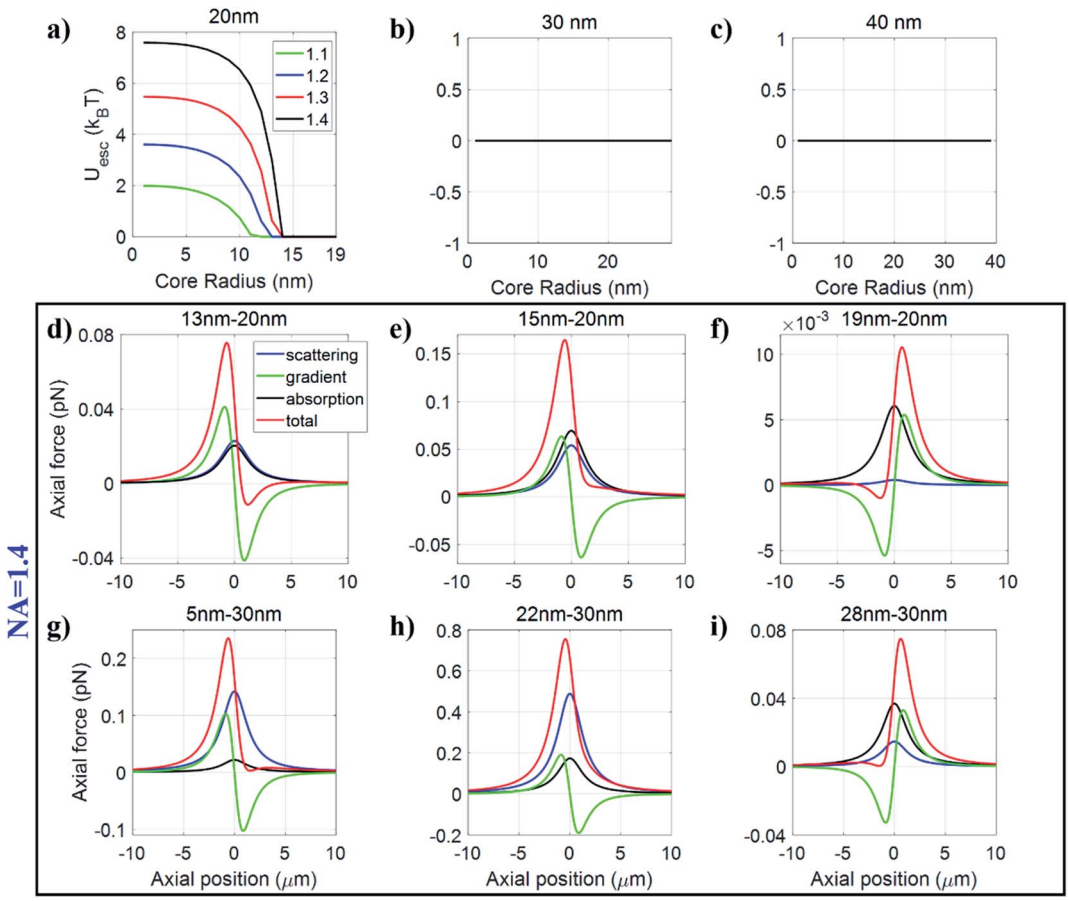

Fig. 3 Plots of the escape potential against core radius by fixing the shell radius to (a) 20 nm, (b) 30 nm, and (c) 40 nm for polystyrene–silver nanoparticles. Plots of trapping force/potentials along the axial direction for (d) 13–20 nm, (e) 15–20 nm, (f) 19–20 nm, (g) 5–30 nm, (h) 22–30 nm, and (i) 28–30 nm polystyrene–silver nanoparticles under CW excitation at 100 mW average power for fixed NA 1.4.

conditions according to Fig. S2a,† which is a promising advantage of using hybrid nanoparticles over conventional nanoparticles for stable trapping. Hence, depending on the requirement, choosing an accurate combination of core and shell size can help to give stable trapping.

Further, we show similar analysis for polystyrene–silver nanoparticles by varying the core radius for a fixed shell radius at 100 mW average power under CW excitation for different NA. From Fig. 3, it can be observed that if we fix the shell radius to 20 nm, the polystyrene core can be varied up to 14 nm, 13 nm, 12 nm, and 11 nm for NA = 1.1, 1.2, 1.3, and 1.4 respectively for achieving a stable trap. For a 20 nm shell, the value of U_{esc} decreases with an increase in the radius of the polystyrene core. This is because with an increase in the core size, the effects of absorption and scattering forces become prominent, due to which the absorption force is enhanced more than the scattering force, and the resulting destabilization can be seen from Fig. 3d and e. Quite interestingly, we observe that for 19–20 nm (polystyrene–silver) particle size, gradient force shows a repulsive nature. Hence, the overall force acting on the particle is also repulsive. On account of decreasing the shell thickness, the polarizability due to the shell layer also decreases and after a specific limit ($n_s^2 - n_w^2 < 0$), the sign of the real part of the polarizability reverses; hence gradient force shows a repulsive nature as shown in Fig. 3f. Further, Fig. 3b and c show the variation of the escape potential with varying core radius when we fix the shell radius to 30 nm and 40 nm. No stable trapping is observed, which is similar to the case of conventional particles because of increased scattering and absorption forces for bigger sized particles. For example, when the core radius is 5 nm, and the shell radius is either 30 nm or 40 nm, we can observe three distinct causes for the destabilization of the trap as we increase the size of the core: initially, the scattering force dominates over both gradient and absorption force. With the further increase, the absorption force exceeds the scattering force, and at 28–30 nm particle size, in addition to this, the gradient force shows the reversal nature of force due to negative polarizability as discussed above and shown in Fig. 3g–i.

Next, we fixed the polystyrene core-radius and varied the metal shell radius and observed that if we fix the core radius of polystyrene to 5 nm, we can trap the particle with the shell radius up to 22 nm, 23 nm, 25 nm, and 27 nm, corresponding to NA = 1.1, 1.2, 1.3, 1.4 as shown in Fig. 4. In this case, initially, for a small-sized hybrid particle, the gradient force dominates over both scattering and absorption forces (Fig. 4d), resulting in stable trapping but a further increase in the particle size or shell

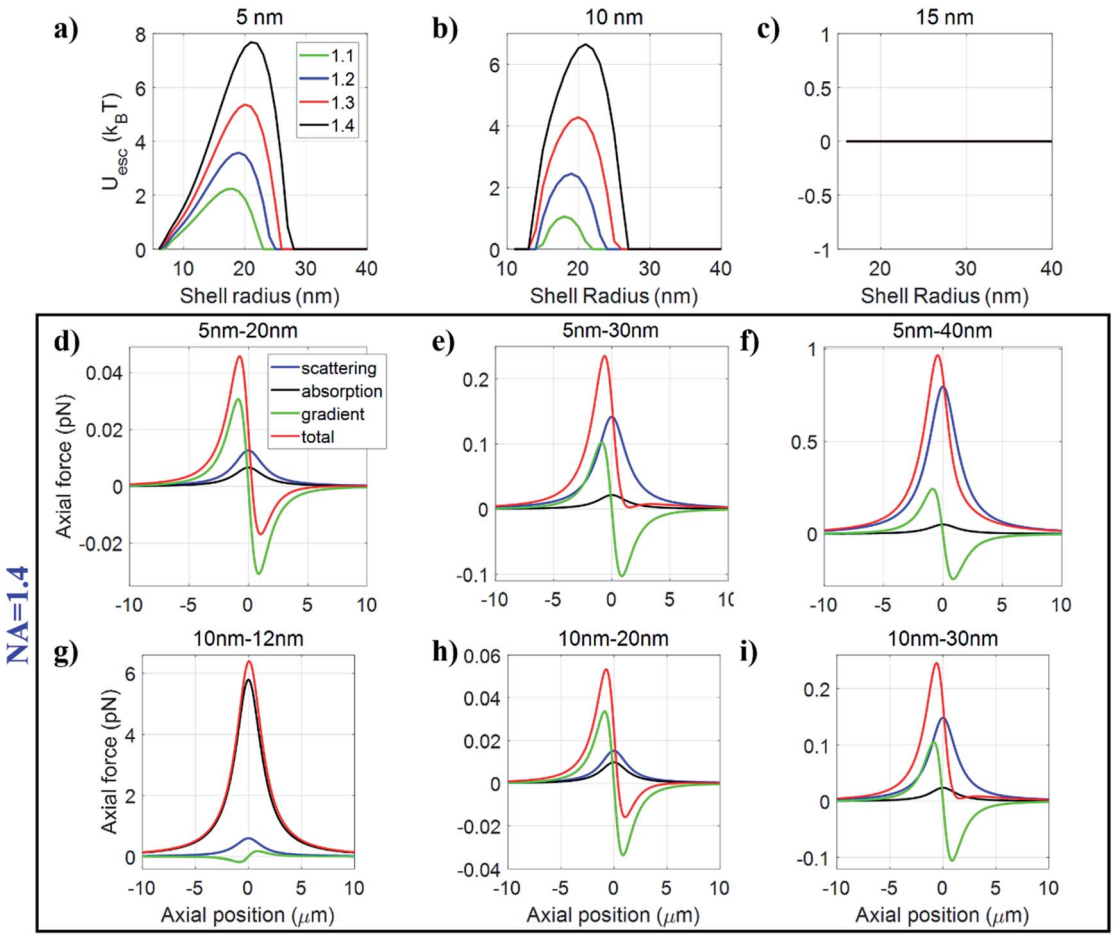

Fig. 4 Plots of the escape potential against shell radius by fixing the core radius to (a) 5 nm, (b) 10 nm, and (c) 15 nm for polystyrene–silver nanoparticles. Plots of trapping force/potentials along the axial direction for (d) 5–20 nm, (e) 5–30 nm, (f) 5–40 nm, (g) 10–12 nm, (h) 10–20 nm, and (i) 10–30 nm polystyrene–silver nanoparticles under CW excitation at 100 mW average power for fixed NA 1.4.

radius results in destabilizing of the trap (Fig. 4e and f). When the core radius is fixed to 10 nm, and the shell thickness is less than 4 nm, the absorption force dominates over scattering and gradient forces, and gradient force shows reverse behavior because the polarizability of the shell layer is less than the surrounding medium—consequently, the total force acting on the particle results in destabilizing the trap (Fig. 4g). A further increase in the shell thickness results in a more stabilized trap due to a fine balance between all three forces (Fig. 4h). However, if the shell thickness is more than 20 nm, the trap gets destabilized due to the dominance of the scattering force over both gradient and absorption forces (Fig. 4i). Thus, there is an optimum size range in which particles can be stably trapped. If the particle size is less than that of this region, then the absorption force is responsible for destabilizing. Beyond this size range, the scattering force is responsible for destabilizing the trap. However, when we increase the core radius to 15 nm, no stable trapping is achieved for any particle size due to the combined destabilising effect of both scattering and absorption forces (Table 1).

Pulsed excitation

Fig. S4† shows the variation of escape potential by fixing the shell radius and varying the core radius for silver–polystyrene nanoparticles under pulsed excitation. Fig. S4a–c† show the variation of the core radius at three different fixed shell radii 20 nm, 30 nm, and 40 nm at 100 mW average power. Under pulsed excitation, nonlinearity contributes significantly, leading to significant enhancement in scattering and absorption forces compared to the case of CW excitation. The destabilization is strongest for bigger sized particles. For instance, the 20–40 nm (silver–polystyrene) particles can be trapped under CW excitation but not under pulsed excitation for fixed NA = 1.4. On the other hand, for small-sized particles, pulsed excitation can trap much better than CW excitation. For example, the 5 nm–30 nm (silver–polystyrene) particles have $U_{esc} \sim 4k_BT$ under CW excitation, however, under pulsed excitation $U_{esc} \sim 7k_BT$. This is a clear indication that pulsed excitation is advantageous over CW excitation for smaller sized particles but less favorable for bigger size particles under similar conditions.

Following this, we also studied the variation of average power by fixing the shell radius as 20 nm and varying the core radius as optical nonlinearity is strongly dependent on the average power. For smaller core (silver) particles, we observed that at high average powers (300 mW or 500 mW), there is an appearance of a second potential well in addition to the one already present.[31,32] Such behavior was not observed in the case of dielectric particles and we traced the origin of this phenomenon due to the splitting observed in the absorption force and in the imaginary part of polarizability. This splitting behavior may be attributed to the plasmonic and heating effects that are absent in the case of dielectric particles which results in an initial decrease in U_{esc} with increasing core radius followed by a subsequent increase shown in Fig. S4d–f.†

Fig. S5† shows the variation of escape potential by fixing the core radius and varying the shell radius for silver–polystyrene nanoparticles under pulsed excitation. Fig. S5a–c† show the escape potential against variation of the shell radius at three different fixed core radii 5 nm, 10 nm, and 15 nm at 100 mW average power. Under pulsed excitation, the escape potential first increases with increasing overall particle size along the axial direction, followed by a maximum and then decreases. However, under CW excitation, the escape potential continuously increases with increasing (overall) particle size when the core radius is 5 nm. Comparing the plots in Fig. S5,† we can see that the maximum in the curve becomes less defined on increasing the size of the silver core from 5 nm to 15 nm. This is because the nonlinear contribution is dependent on the size proportionality of the core and the shell and with increasing contribution from the metal, the magnitude of the escape potential diminishes rapidly. As seen in Fig. S3,† in the linear case, there is no well-defined maximum for the silver–polystyrene nanoparticles, which means that under CW excitation, the corresponding optimal particle-size for most stable trapping is much higher, for a fixed average power.

The inclusion of nonlinearity brings about a shift in the peak for the case of polystyrene, which indicates that even smaller particles can be trapped with better efficiency. So, it can be concluded that for a fixed power, nonlinear contributions must be included to precisely predict the optimal particle-size for stable trapping. This is particularly important for particles with high nonlinear refractive indices like polystyrene and silver. The appearance of maxima can be explained by considering the fact that at small sizes, the contribution of scattering and absorption forces is comparatively less, but it contributes as the particle size increases, first stabilizing the trap and then destabilizing as the size increases further. A peak in the curve marks this change from stabilizing to destabilizing behavior. The same behaviour is observed when the core radius is smaller in size, so that polystyrene effects dominate over silver because the outer layer is polystyrene, but with increasing core radius, the effect of silver also contributes significantly. After a threshold particle-size, the trap becomes unbound. Another

Table 1 The parameters used in simulations for trapping force and potentials

Description	Symbol	Expression/value
Central wavelength	λ	800 nm
Speed of light	c	3×10^8 m s^{-1}
Repetition rate	f	76 MHz
Pulse width	τ	120 fs
Background permittivity[36]	ε_∞	2.5
Plasma frequency[36]	ω_p	1.37×10^{16} Hz
Collision damping frequency[36]	γ_c	3.2258×10^{13} Hz
Linear RI of water[37]	n^w	1.329
Linear RI of polystyrene[37]	n^p	1.578
2nd order NRI of water[38]	n_2^w	2.7×10^{-20} m^2 W^{-1}
2nd order NRI of silver NP[39]	n_2^s	7.5×10^{-20} m^2 W^{-1}
4th order NRI of silver NP[39]	n_4^s	5×10^{-35} m^4 W^{-2}
6th order NRI of silver NP[39]	n_6^s	7.5×10^{-51} m^6 W^{-3}
2nd order NAC of silver NP[39]	σ_2^s	13.2×10^{-14} m W^{-1}
4th order NAC of silver NP[39]	σ_4^s	9×10^{-29} m^3 W^{-2}
6th order NAC of silver NP[39]	σ_6^s	7×10^{-44} m^5 W^{-3}

feature observed is that including nonlinearity leads to a strong dependency on the average power for achieving stable trapping. Under pulsed excitation, there is a shift of maxima towards a smaller particle size, indicating that by increasing the power, it is possible to trap even smaller particles. However, under CW excitation, unlike pulsed excitation, there is no shift in peaks (with respect to particle-size) with the change in power because trap stiffness is linearly dependent on power.

Fig. 5 shows the variation of the escape potential by fixing the shell radius and varying the core radius for polystyrene–silver nanoparticles under pulsed excitation. Fig. 5a–c show the variation of the core radius at three different fixed shell radii 20 nm, 30 nm, and 40 nm. It is evident that if the shell material is silver, then particles with overall size of more than 27 nm cannot be trapped, as discussed above. Fig. 5d–f show the trapping force along the axial direction, and for 10–20 nm particle size, where absorption force dominates over the gradient and scattering force, but still resultant force shows confinement along the axial direction. Further increasing the core radius results in splitting of the absorption force curve which regains confinement again. In other words, we can say that with increasing core radius, the optical trap first stabilizes and then becomes unbound, and after a certain particle size, it again stabilizes. An interesting point here is that force acting on the 19–20 nm particles is repulsive under CW excitation while it is attractive under pulsed excitation under similar conditions. This means that the 19–20 nm particles cannot be trapped under CW excitation, but they can be trapped under pulsed excitation due to the significant contribution of nonlinear effects since the optical nonlinearity is strongly dependent on the average power. We further explore the effect of average power on trapping efficiency as shown in Fig. 5g–i and observe that for smaller sized particles, increasing power destabilizes the trap, however, bigger sized particles which cannot be trapped at low average power, can be trapped at

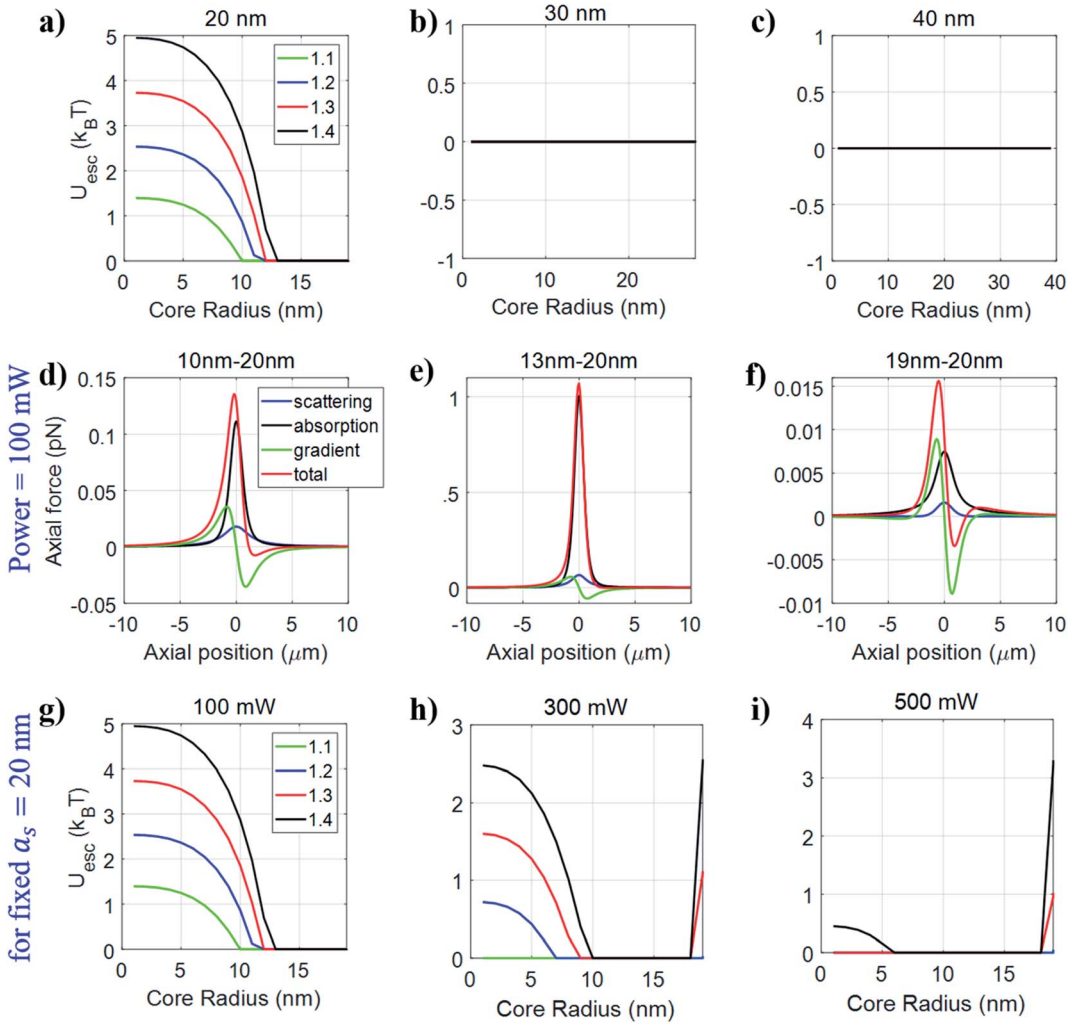

Fig. 5 Plots of the escape potential against core radius by fixing the shell radius to (a) 20 nm, (b) 30 nm, and (c) 40 nm for polystyrene–silver nanoparticles under pulsed excitation at 100 mW average power. Plots of trapping force/potentials along the axial direction for (d) 10–20 nm, (e) 13–20 nm, and (f) 19–20 nm polystyrene–silver nanoparticles under pulsed excitation at 100 mW average power for fixed NA 1.4. Plots of the escape potential against core radius by fixing the shell radius to 20 nm (g) 100 mW, (h) 300 mW, and (i) 500 mW average power for polystyrene–silver nanoparticles under pulsed excitation.

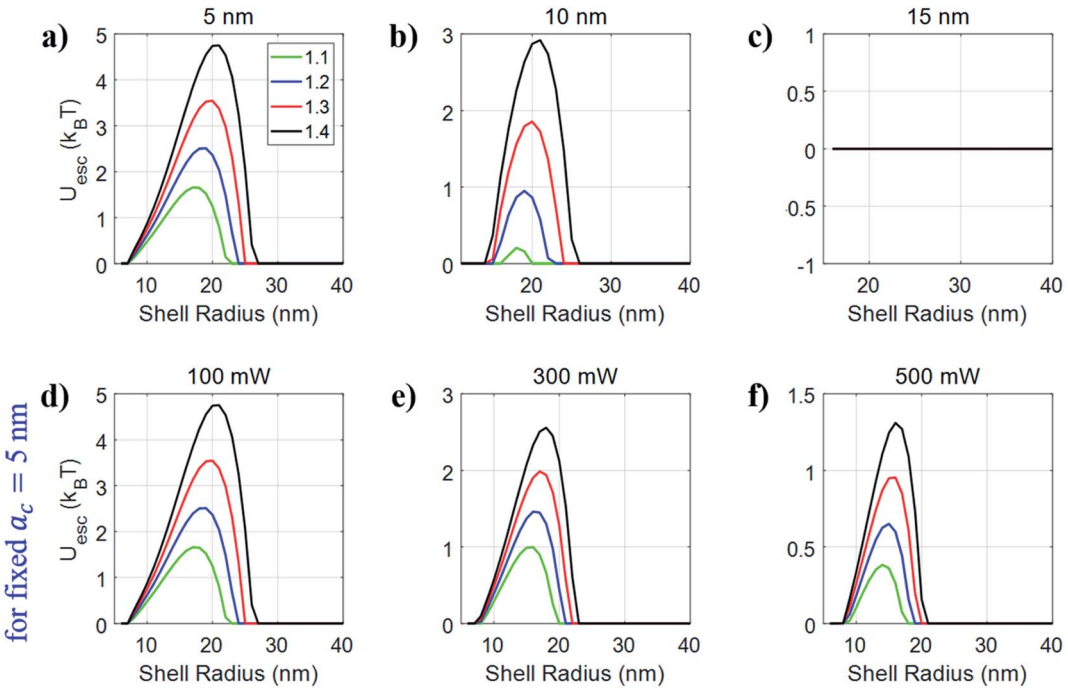

Fig. 6 Plots of the escape potential against shell radius by fixing the core radius to (a) 5 nm, (b) 10 nm, and (c) 15 nm at 100 mW average power, and (d) 100 mW, (e) 300 mW, and (f) 500 mW for the fixed core radius of 5 nm for silver–polystyrene nanoparticles under pulsed excitation.

high average power. For example, 18–20 nm particles cannot be trapped at 100 mW average power but can be trapped at 500 mW average power. However, 10–20 nm particles can be trapped at 100 mW average power but cannot be trapped at 500 mW average power. So, depending on the particle size, we should cautiously choose the average power to obtain stable trapping.

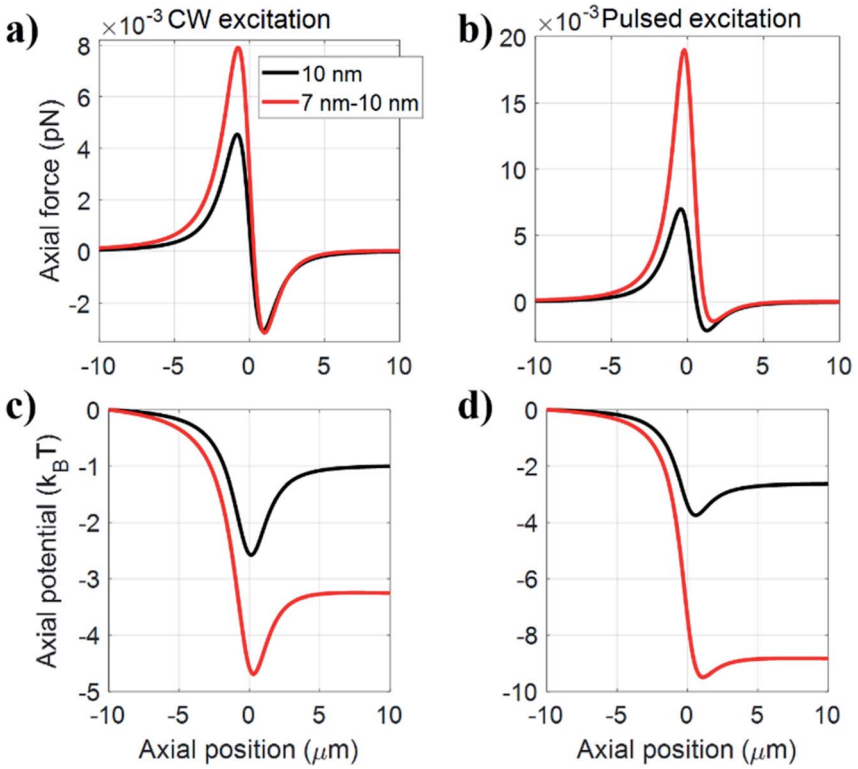

Fig. 7 Plots of trapping (a) force, (c) potential under CW excitation and (b) force, (d) potential under pulsed excitation along the axial direction for conventional silver and hollow core silver nanoparticles at 100 mW average power for fixed NA 1.4.

Fig. 6 shows the variation of the escape potential by fixing the core radius and varying the shell radius for polystyrene–silver nanoparticles under pulsed excitation. Fig. 6a–c show the variation of the shell radius at three different fixed core radii 5 nm, 10 nm, and 15 nm at 100 mW average power. If the core (metallic) radius is more than 15 nm, no stable trapping is observed, as discussed in Fig. 4 under CW excitation. The trend of the curve is similar to that under CW excitation, but increasing average power narrows down the region of stable trapping in terms of particle size, as shown in Fig. 6d–f. This is because with increasing power, the contribution of the nonlinear refractive index increases more than the linear refractive index, which elevates the absorption and scattering forces. So, for small-sized particles, the absorption force increases significantly, and is responsible for destabilizing the optical trap. For bigger sized particles, the rapidly increasing scattering force is responsible for destabilizing the trap. In between both the limiting cases, there is a region where scattering, gradient, and absorption forces balance each other in such a way that stable trapping can be achieved.

Hollow nanoparticles

As the name suggests, these particles have a hollow space within them and have vast application in the medical field, especially, for drug delivery purposes utilizing the large fraction of empty space for loading and controlled release of target-specific materials such as drugs, genes, biological molecules, *etc.* The increased surface area of these particles opens up new possibilities in high energy storage and conversion, sensing, and catalysis.[39] In previous studies, the advantage of using pulsed excitation to reverse the direction of trapping of hollow dielectric particles was theoretically shown.[34,35] Fig. 7 shows the trapping force/potential along the axial direction, compared among conventional (silver) and hollow-core silver nanoparticles at 100 mW average power for fixed NA 1.4 under both CW and pulsed excitation. On comparison of the force/potential for 10 nm silver nanoparticles with 7 nm−10 nm (air–silver) hollow nanoparticles, we observe that hollow-core nanoparticles show significant enhancement in force relative to conventional nanoparticles. This enhancement is further increased under pulsed excitation.

Conclusion

From the studies presented here on the diverse trapping behavior of conventional, hybrid and hollow-core nanoparticles under both CW and femtosecond pulsed excitations, it is evident that hybrid and hollow-core nanoparticles are advantageous over conventional nanoparticles, in particular under pulsed excitation. The findings show how one can simultaneously optimize the design of materials as well as laser parameters that would result in the best trapping conditions for facile manipulation of these hybrid and hollow-core particles and envision far-reaching applications.

Author contributions

AD and SSN carried out the numerical simulations and contributed equally to this work supervised by AKD. All authors participated in the writing of the manuscript and discussed and commented on the final version of this manuscript.

Conflicts of interest

The authors declare no conflict of interest.

Acknowledgements

This work was funded by SERB, DST (Early Career Research Award, Grant No: ECR/2016/000467) and IISER Mohali (Start-up Grant). AD, SSN and SY thank IISER Mohali, DST (INSPIRE) and UGC, respectively, for providing fellowships.

References

1 A. Ashkin, J. M. Dziedzic, J. E. Bjorkholm and S. Chu, Observation of a single-beam gradient force optical trap for dielectric particles, *Opt. Lett.*, 1986, **11**(5), 288–290.
2 J. E. Molloy and M. J. Padgett, Lights, action: optical tweezers, *Contemp. Phys.*, 2002, **43**(4), 241–258.
3 A. Ashkin, Acceleration and trapping of particles by radiation pressure,", *Phys. Rev. Lett.*, 1970, **24**, 156.
4 A. Ashkin, Optical trapping and manipulation of viruses and bacteria, *Science*, 1987, **235**, 1517–1520.
5 A. Ashkin and J. M. Dziedzic, Internal cell manipulation using infrared laser traps, *Proc. Natl. Acad. Sci.*, 1989, **86**, 7914–7918.
6 A. Ashkin, Optical trapping and manipulation of neutral particles using lasers: a reprint volume with commentaries, *World Scientific*, 2006, 125–126.
7 S. M. Block, D. F. Blair and H. C. Berg, Compliance of bacterial flagella measured with optical tweezers, *Nature*, 1989, **338**, 514–518.
8 A. Rohrbach, Stiffness of optical traps: quantitative agreement between experiment and electromagnetic theory, *Phys. Rev. Lett.*, 2005, **95**, 168102.
9 K. Sasaki, M. Koshioka, H. Misawa, N. Kitamura and H. Masuhara, Optical trapping of a metal particle and a water droplet by a scanning laser beam, *Appl. Phys. Lett.*, 1992, **60**(7), 807–809.
10 B. A. Kemp, T. M. Grzegorczyk and J. Au Kong, Optical Momentum Transfer to Absorbing Mie Particles, *Phys. Rev. Lett.*, 2006, **97**, 133902.
11 K. Svoboda and S. M. Block, Optical trapping of metallic Rayleigh particles, *Opt. Lett.*, 1994, **19**(13), 930–932.
12 P. M. Hansen, V. K. Bhatia, N. Harrit and L. Oddershede, Expanding the Optical Trapping Range of Gold Nanoparticles, *Nano Lett.*, 2005, **5**(10), 1937–1942.
13 L. Bosanac, T. Aabo, P. M. Bendix and L. B. Oddershede, Quantitative Optical Trapping of Single Gold Nanorods, *Nano Lett.*, 2008, **8**(5), 1486–1491.

14 F. Hajizadeh and S. N. S. Reihani, Optimized optical trapping of gold nanoparticles, *Opt. Express*, 2010, **18**(2), 551–558.
15 K. J. Lee, P. D. Nallathamby, L. M. Browning, C. J. Osgood and X.-H. Nancy Xu, *In Vivo* Imaging of Transport and Biocompatibility of Single Silver Nanoparticles in Early Development of Zebrafish Embryos, *ACS Nano*, 2007, **1**(2), 133–143.
16 A. Chrastina and J. Schnitzer, Iodine-125 radiolabeling of silver nanoparticles for *in vivo* SPECT imaging, *Int. J. Nanomed.*, 2010, **5**, 653–659.
17 S. Prabhu and E. K. Poulose, Silver nanoparticles: mechanism of antimicrobial action, synthesis, medical applications, and toxicity effects, *Int. Nano Lett.*, 2012, **2**, 32.
18 A. Travan, C. Pelillo, I. Donati, E. Marsich, M. Benincasa, T. Scarpa, S. Semeraro, G. Turco, R. Gennaro and S. Paoletti, Non-cytotoxic Silver Nanoparticle-Polysaccharide Nanocomposites with Antimicrobial Activity, *Biomacromolecules*, 2009, **10**(6), 1429–1435.
19 B. S. Kim and T. R. Lee, The Development of Smart, Multi-Responsive Core@Shell Composite Nanoparticles, *Nanopart. Technol.*, 2015, 103–115.
20 M. H. Rahaman and B. A. Kemp, Analytical model of plasmonic resonance from multiple core-shell nanoparticles.", *Opt. Eng.*, 2017, **56**, 121903.
21 R. R. Agayan, T. Horvath, B. H. McNaughton, J. N. Ankera and R. Kopelman, Optical manipulation of metal-silica hybrid nanoparticles, *Proc. SPIE*, 2004, **5514**, 502–513.
22 C. Loo, A. Lin, L. Hirsch, M.-H. Lee, J. Barton, N. Halas, J. West and R. Drezek, Nanoshell-enabled photonics- based imaging and therapy of cancer, *Technol. Cancer Res. Treat.*, 2004, **3**, 33–40.
23 L. Zhang, D. A. Blom and H. Wang, Au-Cu_2O core-shell nanoparticles: a hybrid metal- semiconductor heteronanostructure with geometrically tunable optical properties, *Chem. Mater.*, 2011, **23**, 4587–4598.
24 J. C. Cordova, D. N. Reinemann, D. J. Laky, W. R. Hesse, S. K. Tushak, Z. L. Weltman, K. B. Best, R. Bardhan and M. J. Lang Bioconjugated, Core–Shell Microparticles for High-Force Optical Trapping, *Part. Part. Syst. Charact.*, 2018, **35**, 1700448.
25 R. G. Chaudhuri and S. Paria, Core/Shell Nanoparticles: Classes, Properties, Synthesis Mechanisms, Characterization, and Applications, *Chem. Rev.*, 2012, **112**, 2373–2433.
26 J.-G. Oh and H. Kim, Synthesis of core–shell nanoparticles with a Pt nanoparticle core and a silica shell, *Curr. Appl. Phys.*, 2013, **13**(1), 130–136.
27 O. Niitsoo and A. Couzis, Facile synthesis of silver core-silica shell composite nanoparticles, *J. Colloid Interface Sci.*, 2011, **354**(2), 887–890.
28 A. Devi and A. K. De, Theoretical investigation on nonlinear optical effects in laser trapping of dielectric nanoparticles with ultrafast pulsed excitation, *Opt. Express*, 2016, **24**(9), 21485–21496.
29 A. Devi and A. K. De, Theoretical estimation of nonlinear optical force on dielectric spherical particles of arbitrary size under femtosecond pulsed excitation, *Phys. Rev. A*, 2017, **96**(2), 023856.
30 A. Devi and A. K. De, Generalized description of the nonlinear optical force in laser trapping of dielectric nanoparticles, *Phys. Rev. Res.*, 2020, **2**, 043378.
31 A. Devi, S. N. Nair and A. K. De, Disappearance and reappearance of optical trap for silver nanoparticles under femtosecond pulsed excitation: A theoretical investigation, *Europhys. Lett.*, 2019, **126**, 28002.
32 S. Yadav, A. Devi and A. K. De, Synergistic effect of Fano-resonance and optical nonlinearity in laser trapping of silver nanoparticles, *Phys. Rev. A*, 2020, **102**, 043511.
33 P. Polimeno, F. Patti, M. Infusino, J. Sánchez, M. A. Iatì, R. Saija, G. Volpe, O. M. Maragò and A. Veltri, Gain-Assisted Optomechanical Position Locking of Metal/Dielectric Nanoshells in Optical Potentials, *ACS Photonics*, 2020, **7**, 1262–1270.
34 A. Devi and A. K. De, Harnessing optical nonlinearity to control reversal of trapping force: A theoretical investigation, *J. Opt.*, 2019, **21**(1–8), 065502.
35 A. Devi and A. K. De, Generalized Lorenz-Mie theory for the reversal of optical force in a nonlinear laser trap, *Phys. Rev. A*, 2020, **102**, 023509.
36 M. Dienerowitz, Plasmonic effects upon optical trapping of metal nanoparticles, Thesis Doctor of Philosophy, University of St. Andrews, UK, 2010.
37 http://refractiveindex.info/.
38 M. J. Weber, *CRC Handbook of Optical Material*, CRC Press, Boca Raton, FL, 2003, vol. III.
39 D. Rativa, R. E. de Arauno and A. S. L. Gomes, One photon nonresonant high-order nonlinear optical properties of silver nanoparticles in aqueous solution, *Opt. Express*, 2008, **16**(23), 19244–19252.
40 W. I. Abdel-Fattah and G. W. Ali, On the anti-cancer activities of silver nanoparticles, *J. Appl. Biotechnol. Bioeng.*, 2018, **5**(2), 001165.